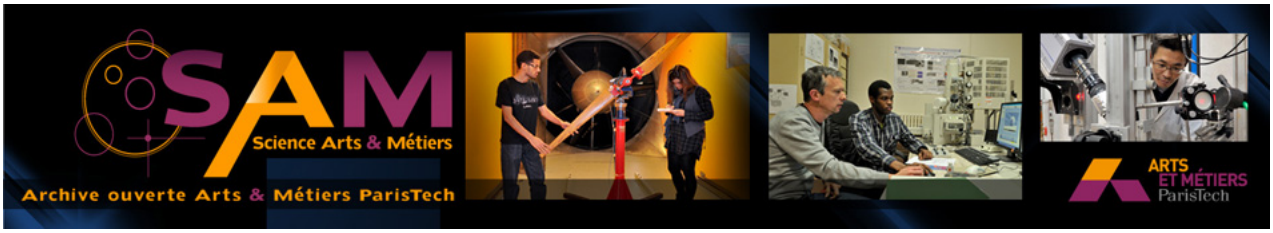

Very high cycle fatigue of copper: Evolution, morphology and locations of surface slip markings

N.L. Phung [a], V. Favier [a,*], N. Ranc [a], F. Valès [a], H. Mughrabi [b]

[a] Arts et Métiers ParisTech, PIMM UMR CNRS 8006, 151 Bd de l'Hôpital, 75013 Paris, France
[b] Department of Materials Science & Engineering, University of Erlangen-Nürnberg, Martensstr. 5, 91058 Erlangen, Germany

A B S T R A C T

The surfaces of commercially pure polycrystalline copper specimens subjected to interrupted 20 kHz fatigue tests in the very high cycle fatigue regime were investigated. The stress amplitude needed to form the early slip markings was found twice lower than the stress amplitude required to fracture which confirmed the results obtained by Stanzl-Tschegg et al. (2007). Three types of slip markings were classified according to their morphology and their location in the polycrystalline material. They are compared to slip markings observed during fatigue tests at frequencies lower than 100 Hz and numbers of cycles lower than 10^7. For 20 kHz fatigue tests, stress amplitudes ranging from 45 MPa to 65 MPa produce straight and long early persistent slip markings located along twin boundaries. Stress amplitudes lower than 45 MPa produce clusters of fine early persistent slip markings mainly located at triple junctions.

Keywords:
Very high cycle fatigue
Persistent slip bands
Grain boundaries
Strain localization
Fatigue limit

1. Introduction

There is currently a growing demand to investigate the very high cycle fatigue (VHCF) regime (higher than 10^7 cycles) to improve the reliability of design calculations and to extend the service lifetimes of some components such as engines. The shape of the S–N curve (plot of stress versus number of cycles to failure) varies with the material [1]. The hardest materials were found to exhibit a gradual decrease of the fatigue resistance with increasing number of cycles, whereas the softest alloys were found to present a plateau from 10^7 up to 10^9–10^{10} cycles [2]. Titanium and tantalum [3] and aluminium [4] exhibit a decrease of the fatigue resistance at a constant rate from 10^4 up to 10^8 cycles. The S–N curve for pure copper displays two slopes: the decrease of the fatigue resistance is stronger from 10^4 up to 10^7 cycles than from 10^7 up to 10^9 cycles [5–8]. All these results demonstrated that failure could occur beyond 10^7 cycles. However, the reason why such discrepancy as far as the VHCF response with regard to material is concerned is not clearly understood. Mughrabi [8] suggested distinguishing two classes of metallic materials when they are loaded in the VHCF regime: type I materials are pure ductile single-phase metals containing no extrinsic internal defects; type II materials contain internal defects such as precipitates or non-metallic inclusions. Most current studies have focused on the VHCF behavior of type II materials and revealed that, in the transition from high cycle fatigue (HCF) to VHCF, the origins of fatigue failure changed from surface to interior "fish-eye" fracture for instance at non-metallic inclusions [1,7]. For type I materials, only few investigations mainly on copper [9–12] are available regarding the shape of the fatigue life curve and the damage evolution [9–14]. Hessler et al. [9] and Weidner et al. [11] showed that cyclic strain localization in VHCF below the PSB threshold occurs in some form of PSBs. Despite the fact that there seems to be no possibility for the formation of a pronounced PSB structure at very low stress amplitudes, Mughrabi's model suggests that cracks initiate at the surface owing to the accumulation of very small but irreversible plastic deformation over very large number cycles [15]. In this work, the morphology and the location of slip markings observed after fatigue testing in the VHCF regime is clarified for pure copper. To perform experiments up to a very high number of cycles in a reasonable time, ultrasonic equipment at a testing frequency of 20 kHz was used. Three types of persistent slip markings are classified for the first time in terms of the stress amplitude ranges at which they appear predominantly. Slip markings morphology observed at 20 kHz and frequencies lower than 100 Hz are compared. The relationship between the appearance of persistent slip markings and failure is discussed.

* Corresponding author. Tel.: +33 1 44 24 64 07.
E-mail addresses: ngoclam250@yahoo.com (N.L. Phung), veronique.favier@ensam.eu (V. Favier), nicolas.ranc@ensam.eu (N. Ranc), frederic.vales@ensam.eu (F. Valès), hael.mughrabi@ww.uni-erlangen.de (H. Mughrabi).

2. Material and experimental procedure

2.1. Material and specimens

Oxygen-free high-conductivity commercially pure (99.95%) copper was tested. The polycrystalline material was hot rolled and supplied by Griset company. The specimens were extracted from the center of a 14 mm thick plate (Fig. 1). The mean grain size was about 30 μm. The microstructure contains about 0.3 volume fraction of annealed twins. The texture is quasi-isotropic. Fatigue tests were performed using a piezoelectric fatigue machine designed by Bathias and Paris [1]. Cylindrical hourglass shaped specimens were fatigued to get the S–N curve while flat hourglass shaped specimen were designed to carry out surface observations after interrupted fatigue tests. The specimens were designed to run in longitudinal vibration resonance with the piezoelectric machine at 20 kHz. The diameter in the center of the cylindrical specimens was 3 mm. The cross section in the center of the flat specimens was 2 mm thick and 3 mm wide. The dimensions of both specimen types are indicated on Fig. 2. After machining, the specimens were heat treated at 250 °C for 60 min to relieve the residual stress without change of microstructure. After thus thermal treatment, the tensile strength of the material is about 230 MPa. Then, all specimens were mechanically polished and soldered into a screw to attach them to the ultrasonic transducer. Finally, they were electrolytically polished to remove all hardened layers on the specimen surface. As a result, before testing, the specimens were mirror polished and without residual stresses. For all calculations, the Young's modulus was taken equal to 130 GPa [10].

2.2. Experimental procedure

The piezoelectric transducer of the ultrasonic fatigue machine converts an electronic signal into a mechanical displacement. This displacement is amplified via a horn and transmitted to the specimen. It was calibrated at the beginning of each series of tests with a laser extensometer. The displacement was found to be perfectly sinusoidal in the course of time. Assuming pure linear elastic behavior, the strain and stress distributions along the specimen were calculated using a one-dimensional approach (the mechanical variables depend only on x coordinate) in forced vibration regime. The strain was then measured by means of a small strain gage stuck on the specimen surface center to check the calibration. The strain R ratio defined as $\frac{\varepsilon_{min}}{\varepsilon_{max}}$ was -1. In the following, the stress amplitude rather than the strain amplitude is used to define the fatigue test. In hour-glass shaped specimens, the strain and stress amplitudes strongly decrease towards the specimen ends. They are 97% of maximum at places 1.25 mm and 1.5 mm apart from the center for the cylindrical and flat specimens, respectively (Fig. 2). Additional 3D elastic finite element simulations in forced vibration regime, carried out on the hour-glass shaped flat specimen, showed that the stress amplitude at the border of the smallest cross section is slightly greater (∼5%) than the stress amplitude at the center of the cross section.

To get the S–N curve for a number of cycles higher than 10^6, hour-glass shaped cylindrical specimens were continuously fatigued up to failure at various stress amplitudes. Failure occurred when a crack had grown large enough to decrease the natural frequency of the system below the standard operating range (19.5–20.5 kHz) leading to a machine stop. The specimens were cooled with compressed air to avoid self-heating due to intrinsic dissipation. After the fatigue test, they were broken in liquid nitrogen for fracture surface examination.

In addition, fatigue loadings performed on the hour-glass shaped flat specimens were interrupted repeatedly in order to perform surface studies by optical microscopy, scanning electron microscopy (SEM), electron back scattering diffraction (EBSD) technique and atomic force microscopy (AFM) after different numbers of cycles. The stress amplitude range [30–60 MPa] was chosen much smaller than for the S–N curve to observe the early traces of plasticity on the surface specimen. In this stress amplitude range, the specimen heating was found lower than 20 °C so the specimens were not cooled. The morphology of the surface patterns was observed by means of a Hitachi S3600 FEG-SEM. EBSD analyses clarify the places of the plastic markings with regard to the polycrystalline microstructure. AFM was operating directly to the surface specimen (no replica) to keep the details of the roughness. The AFM Vecco nanoscope V was used in tapping mode in ambient air and room temperature. The AFM has a V-shaped Si_3N_4 tip with a spring constant of about 20 N/m of the cantilever beam. The side angle of the tip is 17 nm and the radius of its curvature 8 nm.

3. Results

3.1. S–N curve

The S–N curve of the studied copper obtained by ultrasonic fatigue machine at 20 kHz is shown in Fig. 3. It displays two regimes. In the first regime, failure occurs between 3.6×10^6 and

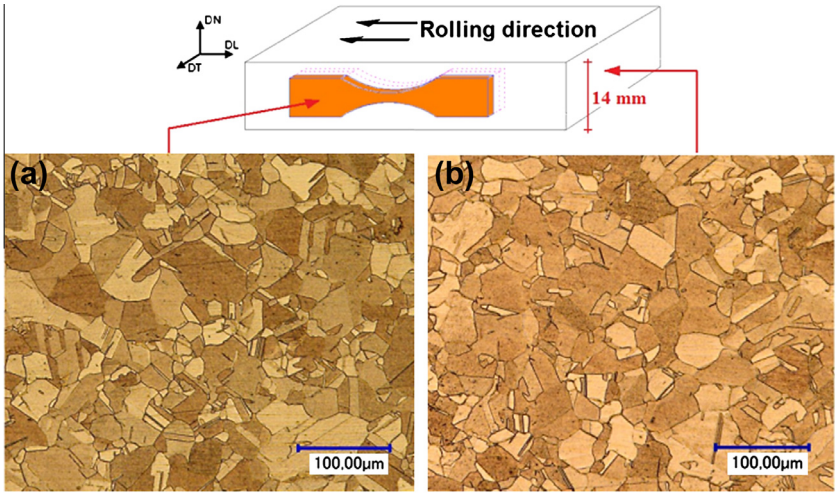

Fig. 1. Polycrystalline pure copper microstructure: cross section (a) in rolling direction and (b) perpendicular to the rolling direction.

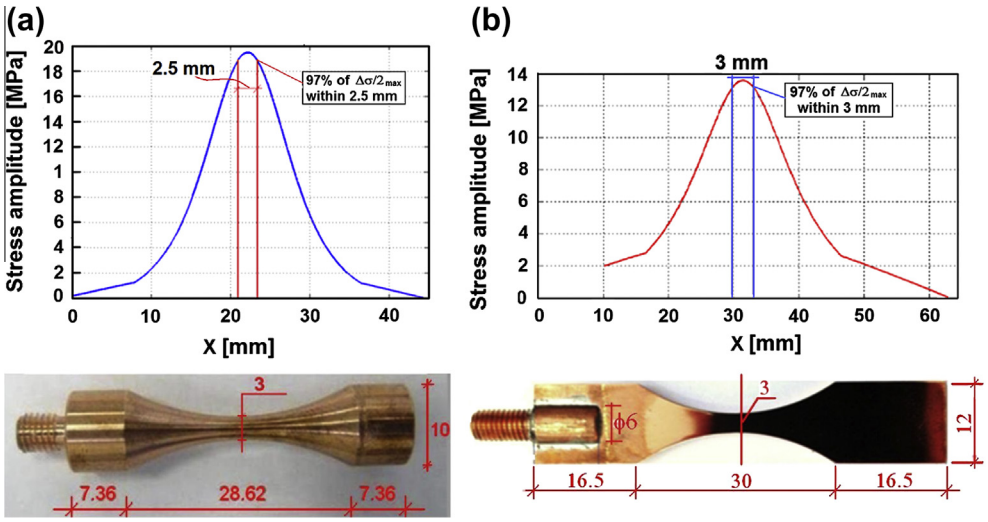

Fig. 2. Ultrasonic fatigue specimens and stress distributions along the specimen axis *x* (a) cylindrical hour glass shaped specimen and (b) flat hour-glass shaped specimen.

5×10^7 cycles with stress amplitude ranging from 115 MPa to 97 MPa. The first regime is associated with the HCF regime. In the second regime, failure takes place at numbers of cycles greater than 5×10^7 cycles. The stress amplitude is lower than 97 MPa. The slope of the S–N curve for more than 10^8 cycles is about 10 times smaller than for less than 10^8 cycles (−0.4 MPa/Log(Number of cycles) versus −5.3 MPa/Log (Number of cycles)). In other words, the number of cycles to failure increases very quickly with decreasing stress amplitude. At a stress amplitude of 91.2 MPa, failure did not occur up to 5.4×10^9 cycles at which the test was stopped. Our results are in good agreement with Stanzl-Tschegg et al.'s experiment results obtained on similar pure polycrystalline copper, especially in the VHCF regime [10,12]. Their results revealed a "fatigue limit at 1×10^{10} cycles" also called "fatigue life threshold" equal to 92.2 MPa.

Fracture surface observations (Fig. 4) showed that the crack initiated at the specimen surface as commonly observed for type I materials [8,14,16]. SEM investigations of the fracture surface and of the surface grains close to the fracture surface reveal that the roughness at the crack initiation zone is very low with regard to the rest of the fracture surface. Crack initiates at a surface grain boundary with one side marked with slip bands while the other side was free of them. Similar results were found by Provan and Zhai [17], Cretigny and Saxena [18] and Mughrabi et al. [19] for pure copper loaded in the LCF regime. It is well-known that crack initiation is intergranular in the LCF regime [17–21]. The fatigue cracks initiate frequently along the large-angle grain boundaries. The HCF regime is the PSB dominated regime. It was commonly admitted that cracks initiate at the interface between the matrix and the PSB in polycrystals as it is in single crystals [19,23]. However many experimental observations showed that PSBs are not only responsible for slip band cracking in PSB, but also induce intergranular cracks [19,24,25]. The latter is promoted by the presence of large-angle grain boundary and the decrease of the stacking fault energy [22]. In the VHCF regime, Stanzl-Tschegg and Schönbauer [12] mentioned that the grain boundaries are the preferred crack nucleation and propagation sites for pure copper loaded at 19 kHz in agreement with the present results.

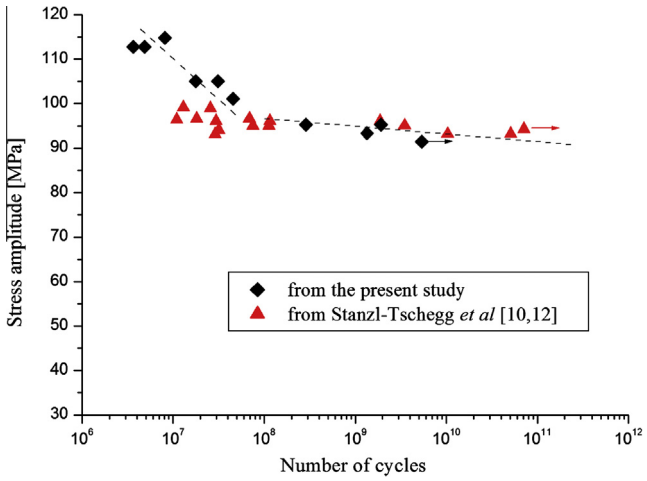

Fig. 3. S–N curve of polycrystalline pure copper obtained from ultrasonic fatigue tests at 20 kHz.

3.2. Slip markings morphology and location

3.2.1. Observation of different types of slip markings

Slip markings on the copper specimen were investigated using SEM and AFM. Three types of markings were distinguished. They are labeled as type I, type II and type III in the following sections (Fig. 5). All the slip markings were shown to be persistent, namely when the surface was electropolished after fatigue, they reappeared at the same sites on the specimen surface when fatigue was resumed. All persistent slip markings are oriented at more or less 45° from the loading direction showing that they are related to the activation of the easiest crystallographic slip systems. They also displayed different features exposed in the following sections.

3.2.2. Characterization of type I persistent slip markings

Figs. 5a and 6 show examples of SEM micrographs of type I persistent slip markings. The latter are long, straight and cross the grains. They gather in family of around ten parallel slip markings. Their roughness is more marked at the grain boundary than in the grain center suggesting that the slip markings initiated at the grain boundary. Fig. 7a illustrates AFM image of type I persistent slip markings. Fig. 7b exhibits the roughness along the white line perpendicular to the persistent slip markings. The peaks are clearly associated with persistent slip markings while the surface is very smooth between them. The height of the persistent slip markings reached 600 nm. The average height deduced from many similar profiles was found about 500 nm. The width of persistent slip markings varies from 0.5 to 3 μm and its average is 1.4 μm. The

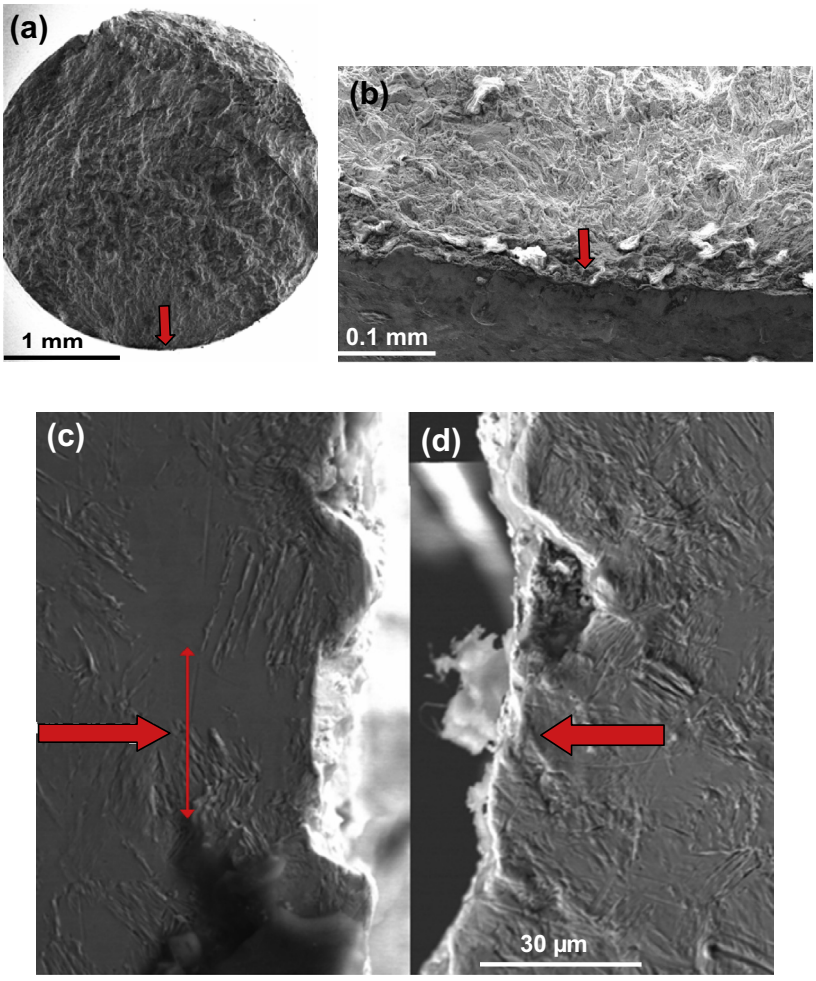

Fig. 4. Fracture specimen at stress amplitude of 105 MPa; $N = 3.1 \times 10^7$ cycles – (a) fracture surface: the crack initiation zone is indicated by the arrow, (b) zoom on the crack initiation zone, (c) specimen surface normal to the fracture, left side, zone free of slip bands, and (d) specimen surface normal to the fracture surface, right side, zone marked with slip bands.

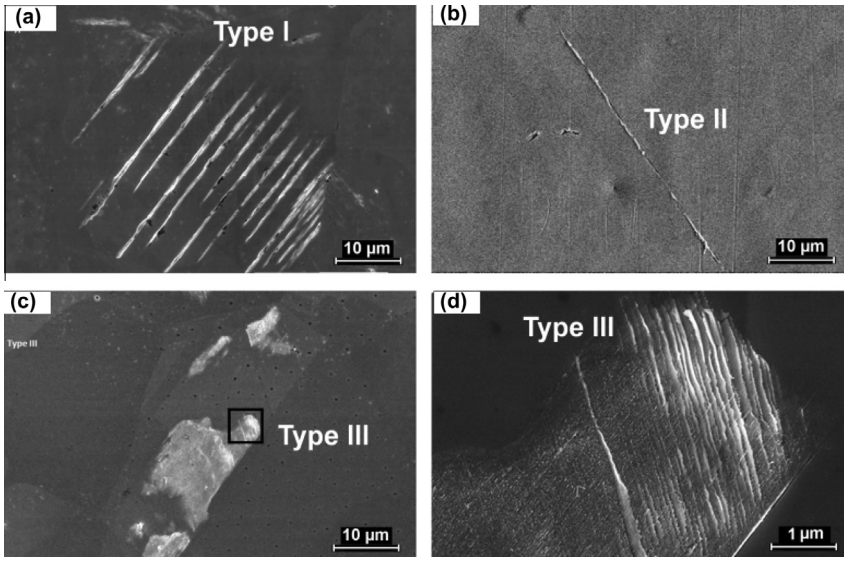

Fig. 5. Three types of persistent slip markings (slip bands) in fatigue – (a) type I at stress amplitude of 86.2 MPa; $N = 5 \times 10^5$ cycles, (b) type II at 57.5 MPa; $N = 10^7$ cycles, (c) type III at stress amplitude of 44 MPa; $N = 4.5 \times 10^8$ cycles, and (d) zoom of c).

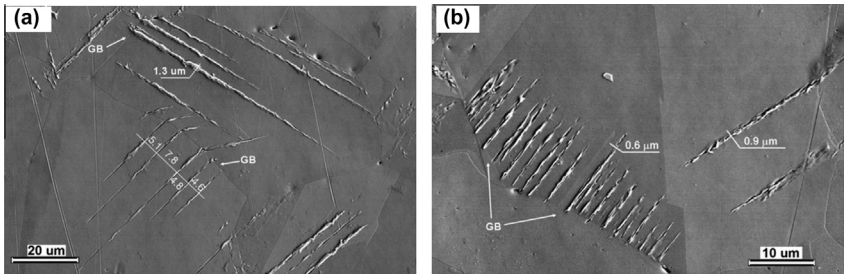

Fig. 6. Type I persistent slip markings at stress amplitude of 89 MPa; $N = 10^6$ cycles – the loading direction is horizontal.

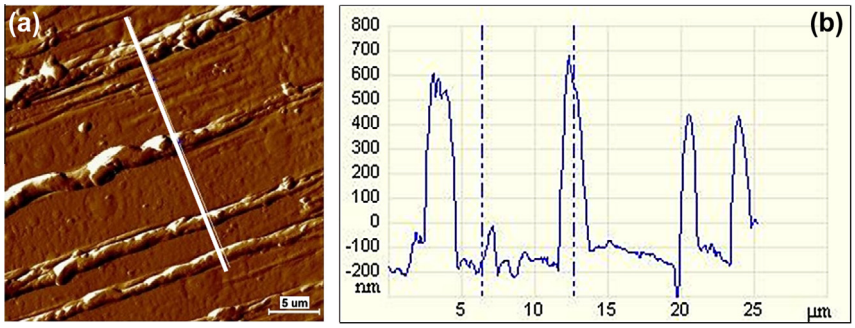

Fig. 7. Surface roughness of type I slip band at stress amplitude of 89 MPa; $N = 10^6$ cycles – (a) AFM image, and (b) surface profile along the line.

distance between slip markings increases with increasing grain size. It is for example about 5–7 µm for the mean grain size of 30 µm (Figs. 6 and 7).

3.2.3. Characterization of type II persistent slip markings

Figs. 5b and 8a show examples of SEM micrographs of type II persistent slip markings. As type I persistent slip markings, they are long and straight but they are isolated and do not cross the grains. EBSD images demonstrate that they are located very near and along grain boundaries and most of the time along and at twin boundaries (Fig. 8b). The affected twin boundaries are oriented at about 45° from the loading direction. The average height of type II is close to type I persistent slip markings height but the maximum height is higher and can reach 1–2 µm depending on the stress amplitude and the number of cycles (Fig. 9) (see Section 3.4).

3.2.4. Characterization of type III persistent slip markings

The early slip markings of type III are invisible under optical microscopy. SEM observations revealed the presence of clusters of very fine slip markings formed inside the grains and near the grain boundaries (Fig. 5c and d). Two slip marking directions were usually observed. The first one is more marked and occupies the majority of the cluster surface. It is very probably associated with the slip band of the primary slip system. The second is less marked and is called secondary slip band (Fig. 10). Fig. 11 shows an AFM image of type III persistent slip markings at a stress amplitude of 50 MPa after 2×10^8 cycles. Their roughness is less than 50 nm. They are located close to large-angle grain boundaries, twin boundaries and preferentially triple junctions.

3.3. Relation between stress amplitude and early persistent slip markings

The appearance of the different types of slip markings depends essentially on stress amplitude. At high stress amplitudes (close to or higher than 92.2 MPa, the fatigue strength at 1×10^{10} cycles), the majority of the early slip markings is of type I (Fig. 12a). The amount of type I persistent slip markings decreases with decreasing stress amplitudes and type II persistent slip markings become more and more numerous. At stress amplitude of 65 MPa, the early persistent slip markings are of type II (Fig. 12b). At very low stress

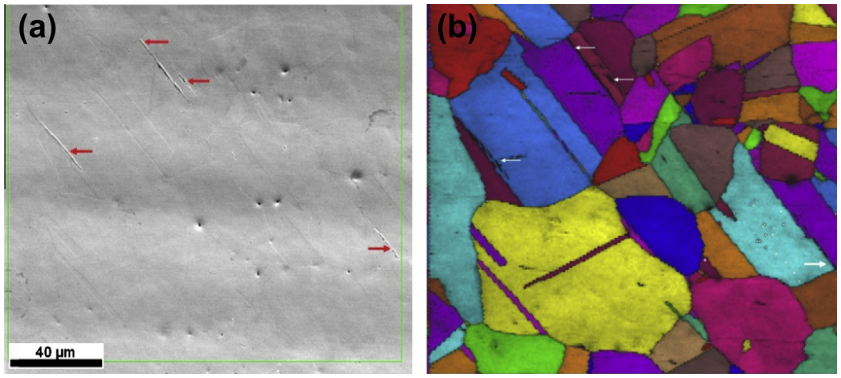

Fig. 8. Type II persistent slip markings (indicated by arrows) at stress amplitude of 57.5 MPa – $N = 10^7$ cycles – (a) SEM image and (b) EBSD analyze at the same zone showing the initiation of type II slip markings SMs at twin boundaries – the loading direction is horizontal.

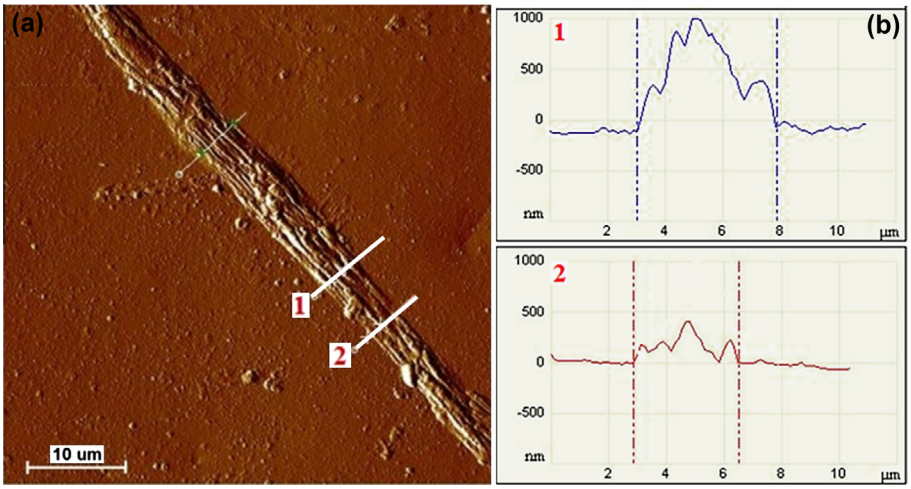

Fig. 9. Surface roughness of a type II persistent slip marking at stress amplitude of 57.5 MPa – $N = 10^7$ cycles – (a) AFM image and (b) surface profiles along the white lines numbered 1 and 2.

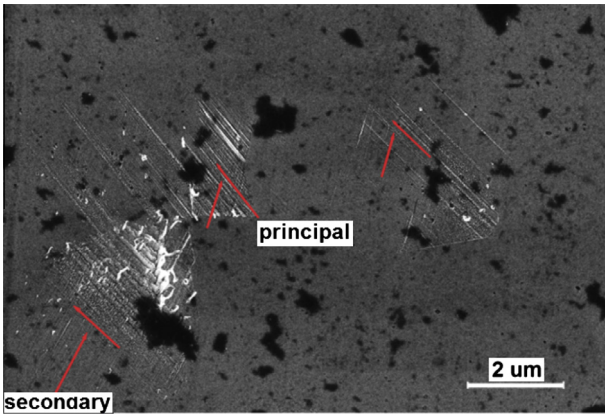

Fig. 10. Type III persistent slip markings at stress amplitude of 48 MPa – $N = 10^8$ cycles oriented along two directions.

amplitudes such as 44 MPa, type III persistent slip markings are predominant and type I persistent slip markings are very rarely observed (Fig. 12c).

The numbers of cycles needed to form the early persistent slip markings and the type of persistent slip markings as a function of the stress amplitude are shown in Fig. 13. At a given stress amplitude, the test was regularly interrupted to observe the slip markings on the specimen surface. In Fig. 13, the experimental data indicate the last observation before slip markings appeared and the next observation when the early slip markings are first detected using SEM. From 62 MPa to 34 MPa, the stress amplitude varies linearly with the logarithm of the number of cycles necessary to form the early slip markings (dashed line in Fig. 13). No slip marking was observed in the region below the dashed line. Above it, persistent slip markings are present at the surface of specimen. Again, our results are in very good agreement with the experimental results obtained by Stanzl-Tschegg et al. [10,12]. All kinds of persistent slip markings (I, II and III) have been reported before [e.g. 13,15]. However, here these three types of early persistent slip markings are classified for the first time in terms of the stress amplitude ranges at which they appear predominantly: the range of stress amplitude higher than 65 MPa is associated with the type I, the range [45–65 MPa] is associated with the type II and the range of stress amplitude lower than 45 MPa with the type III. In particular, it is shown that the persistent slip markings of types II and III are dominant in the VHCF regimes of rather low stress amplitudes.

The S–N curve and the curve for the appearance of the early slip markings are compared in Fig. 14. Up to 10^8 cycles, at a specified number of cycles, the stress amplitude required to break the specimen is twice larger than the stress amplitude needed to form the early slip markings on the specimen surface.

3.4. Evolution of the slip markings morphology and spatial distribution over cycles

When the early type I persistent slip markings appeared on the surface specimen, 5% of grains exhibit them. With increasing the

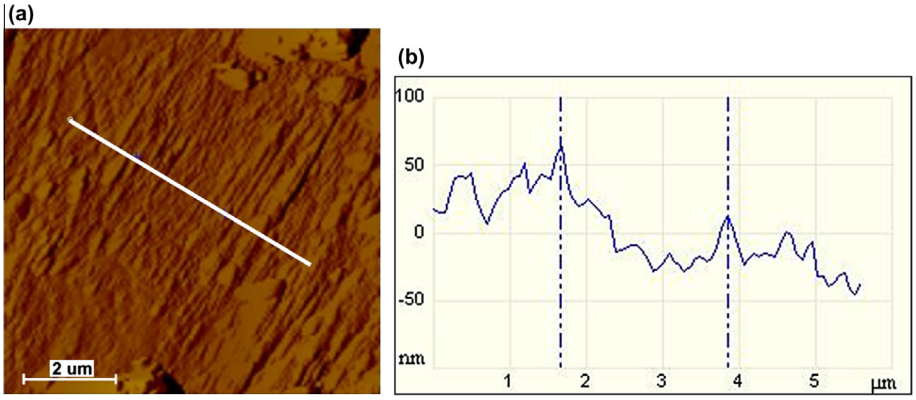

Fig. 11. Surface roughness of type III persistent slip markings at stress amplitude of 50 MPa – $N = 2 \times 10^8$ – (a) AFM image, and (b) surface profile along the white line.

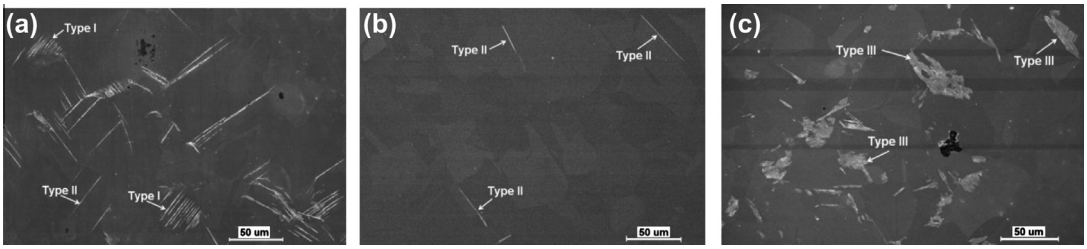

Fig. 12. SEM images of slip band formed at (a) stress amplitude of 90 MPa – $N = 5 \times 10^5$ cycles, (b) stress amplitude of 65 MPa – $N = 10^6$ cycles and (c) stress amplitude of 44 MPa – $N = 4.5 \times 10^8$ cycles.

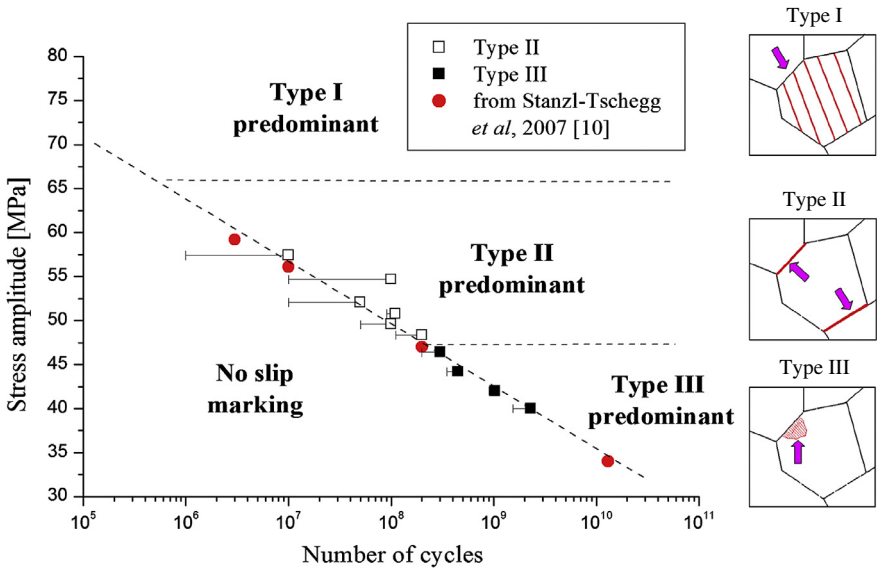

Fig. 13. Stress amplitude needed to form the early slip markings of types I, II and III and scheme of their location as a function of the number of cycles.

numbers of cycles, more parallel slip bands formed inside the grain and the height of the persistent slip markings rises. Concerning the type II persistent slip markings, the majority is formed on twin boundaries. The early type II persistent slip markings are very few, only one slip marking in ~5000 μm^2. The initial persistent slip markings become longer, larger and higher during increasing cycles. AFM measurements showed that the height of type II persistent slip markings can reach 1 μm (Fig. 9a) and sometimes 2 μm. So, type II persistent slip markings can be much higher than type I persistent slip markings. Fig. 15 shows the evolution of a type II persistent slip marking at stress amplitude of 55 MPa after 10^7 cycles, 10^8 cycles and 2×10^8 cycles. Note that the persistent slip marking grows only in the left grain. In addition, some new persistent slip markings appeared 2–3 grains further.

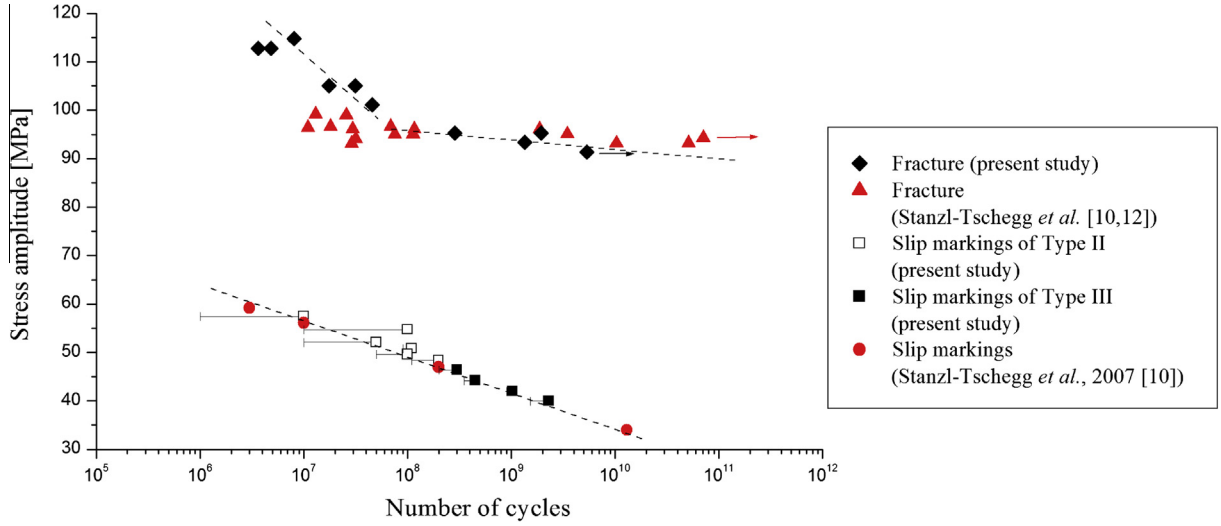

Fig. 14. Stress amplitude–number of cycles for fracture (open and full circles) and for forming the early slip markings (open and full squares).

Concerning the persistent slip markings of type III, when the early slip markings appeared, their quantity is very small as for type II persistent slip markings. With increasing the number of cycles, the clusters of type III persistent slip markings expand, namely new persistent slip markings are observed beside the first ones. Persistent slip markings with other directions are also observed. Fig. 16 shows clusters exhibiting very fine and more pronounced type III persistent slip markings along a twin boundary (Fig. 16a) and at ~30° from a grain boundary (Fig. 16b). In the latter case, the more pronounced persistent slip markings are spaced out 5–10 μm as type I persistent slip markings. A zoom (Fig. 16c) reveals that the persistent slip markings are slightly curved, in contrast to the early type III persistent slip markings. In addition, persistent slip markings having another orientation than the main orientation were detected. These observations suggest that the slip markings type III changes into slip markings type II or type I during increasing cycles due to plastic strain localization mechanisms.

4. Discussion

4.1. Morphology and location of persistent slip markings

Slip markings of type I correspond to the so-called Persistent Slip Bands (PSBs) since their morphology (height and width) and their spatial distribution crossing the grains. They are commonly observed in low and high cycle fatigue regime (see e.g. [18,19,26] for polycrystalline copper). PSBs are usually associated with the ladder-like dislocation structure under the slip marking [27,28].

Persistent slip markings of type II and III are localized at or close to grain and twin boundaries. These observations reveal the key role of grain/twin boundaries acting as stress concentration factors and promoting microplasticity. More precisely, the high majority of the early type II persistent slip markings is located at twin boundaries while triple junctions are preferred sites for type III persistent slip markings. Polak and Vasek [26] observed PSBs similar to type II persistent slip markings at strain amplitudes lower than the "conventional fatigue limit" ($\Delta\varepsilon/2 = 5 \times 10^{-5}$ [29]) in polycrystalline copper. In the same way, Neumann and Tönnessen [24] and Peralta et al. [30] have observed PSBs along twin boundaries oriented at around 45° from the loading direction but not inside the grains at low stress amplitudes. Llanes and Laird [31] showed that twin boundaries promote very early slip and PSB formation. Recently, Man et al. [32] demonstrated the presence of a ladder-like dislocation structure under a slip marking located along a twin boundary after HCF tests in fatigued nickel specimens. The presence of slip bands along twin boundaries was not so much studied in literature. However, more investigations [22,24,25,33] demonstrated the key role of the large-angle grain and twin boundaries on crack initiation. In LCF and HCF, the numerous type I persistent slip markings or equivalently PSBs hide the type II persistent slip markings explaining why few literature results mentioned slip bands along grain and twin boundaries. Besides, the literature results quoted above [20,24–26,31,32] were obtained after symmetrical strain-controlled fatigue tests operated at frequencies below 100 Hz, i.e. much lower than the present frequency (20 kHz). To our knowledge, the key role of twin boundaries on microplasticity initiation was never highlighted for ultrasonic fatigue tests. Comparisons between our results obtained at 20 kHz and literature results obtained at low frequencies [20,24–26,31,32] show that, in both cases, (i) the length, the height, the width and the location of slip markings of type I and II are similar and (ii) the relative amount of the type II slip marking with regard to type I slip band increases with decreasing stress or strain amplitudes. These comparisons suggest that similar mechanisms are responsible for formation of PSBs despite the plastic strain amplitude is much lower and the number of cycles much higher in the VHCF characterized by 20 kHz fatigue tests than in the HCF characterized by low frequency tests. In view of the large height of type II persistent slip markings, it is reasonable to suggest that the type II persistent slip markings could promote intergranular crack initiation at twin boundaries, consistently with the observations. It is worth noticing that Stanzl-Tschegg et al. [10,12] and Weidner et al. [11] discussed the origin of the discrepancy between the PSB thresholds determined by conventional and by ultrasonic fatigue machines. The PSB threshold stress and the stress fatigue limit, measured in ultrasonic tests, are systematically higher than the values found at conventional frequencies. It is attributed to different ramp loading conditions, a strain rate sensitivity effect and/or a time effect related to impurities and diffusion processes.

The morphology of type III persistent slip markings is different from the two others. The type III persistent slip markings are very fine and spread into clusters of closely-spaced parallel bands. This type of persistent slip markings in ductile single-phase metals is rarely mentioned in literature. Stanzl-Tschegg et al. [10] observed parallel 14 nm-height slip bands at triple junctions after 1.05×10^{10} cycles at 45 MPa under fatigue at 20 kHz in similar copper as the present one. Basinski et al. [34] detected very fine, closely-spaced parallel slip bands at low frequency tests on copper single-crystal but after very few number if cycles (lower than 10 and typically one quarter and one half cycles). More pronounced slip markings very rapidly appears to the detriment of the others, very similarly to what we observed in Fig. 15b. Basinski et al. [34] concluded that the deformation associated with the fine slip bands is very homogeneous and probably took place in larger regions without any markings because of recoverable (reversible) slip. Besides, type III persistent slip markings morphology is not so far from the morphology of the so-called shear bands found in underaged alloys [35]. The shear bands are tens of microns in height and spaced about 0.5–2 μm. Generally speaking, literature reviews [22,35] concluded that the distance, the height and the width of the slip markings decrease when planar slip is promoted.

Thus, the type III persistent slip markings very likely result from predominant planar slip of one or two active slip systems. The dislocation interactions between these two systems induce some slip irreversibility leading to markings on the specimen surface.

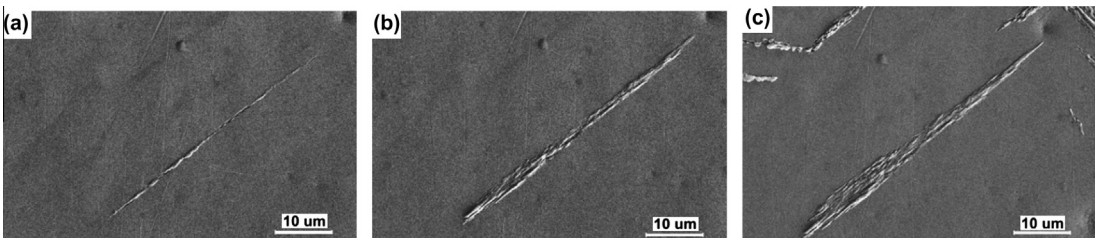

Fig. 15. Evolution of one type II persistent slip marking with numbers of cycles at stress amplitude of 55 MPa – (a) after 10^7 cycles, (b) after 10^8 cycles and (c) after 2×10^8 cycles.

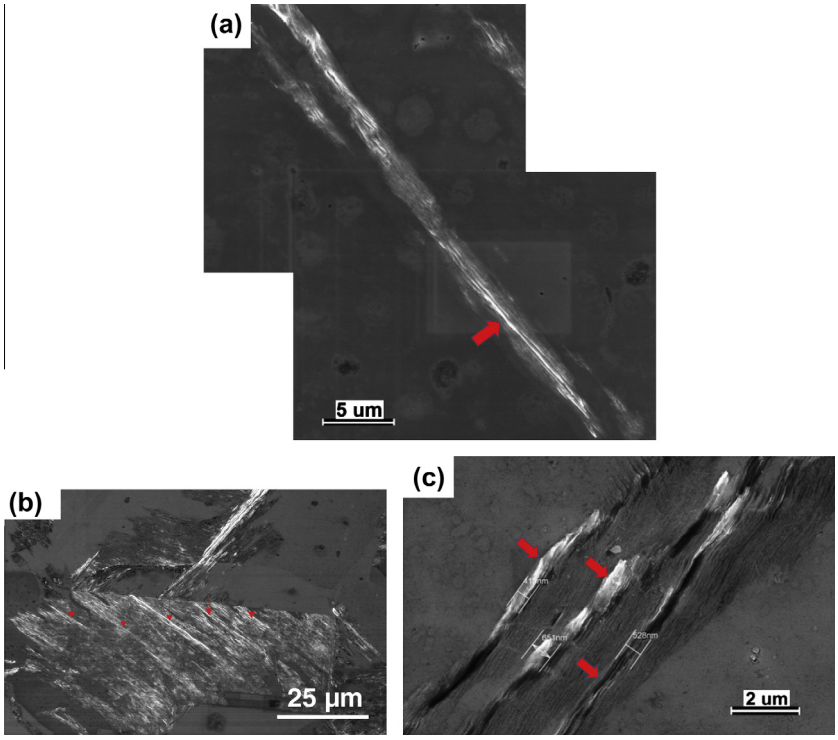

Fig. 16. Plastic strain localization in the cluster of type III persistent slip markings indicated by the arrows – (a) at a twin boundary like type II persistent slip markings at stress amplitude of 48 MPa – $N = 2 \times 10^8$ cycles, (b) close to a grain boundary but pointed at the grain center like type I persistent slip markings at stress amplitude of 44 MPa – $N = 4.5 \times 10^8$ cycles, and (c) similar as (b) but at another place and at higher magnification at which slip markings with another orientation were observed at the top on the micrograph.

Dislocation pile-ups at grain boundaries produce stress concentrations and promote cross slips. As a consequence, dislocation structures form inducing plastic strain localization. This mechanism is consistent with the fact that the type III persistent slip markings change into the type I or II persistent slip markings during increasing cycles. At higher stress amplitudes, the plastic strain localization mechanisms take place much rapidly leading to more pronounced type I persistent slip markings and type II at lower number of cycles.

4.2. Relationship between persistent slip markings appearance and fracture

Results in VHCF demonstrate that when the stress amplitude decreases, the number of cycles to failure and the number of cycles needed to form persistent slip markings increase and no limits are observed. In a previous work [36], a dissipated energy was evidenced at all applied stress ranges, although very small at the lowest stress amplitudes. In addition, the dissipated energy rate was found to always raise during cycles. This result is consistent with the gradual increase of the number of persistent slip markings observed on the specimen surface. The presence of increasing dissipation over cycles indicates that no stabilized cyclic state was reached during the VHCF fatigue tests on copper. In other words, the results show that the fatigue strength of copper (about 93 MPa at 10^{10} cycles) cannot be considered as the fatigue limit from a thermodynamic standpoint, considering that, ideally, the fatigue limit is associated with no change of dissipated and stored energy from one cycle to another. At a given stress amplitude, it is not possible to observe the appearance of the early slip markings and the fracture during the number of cycles reached during experiments. Moreover, the number of cycles for the evolution of slip markings and possibly crack propagation are higher than 10^{12} cycles. These results are in good agreement with [9,10,12]. Stanzl-Tschegg et al. [12] suggested that numerous small cracks do not likely lead to failure below 90 MPa because the cyclic stress intensities remain lower than the stress intensity threshold necessary for crack growth.

5. Conclusions

The surfaces of specimens of commercially pure polycrystalline copper were investigated after 20 kHz fatigue tests in the VHCF regime. The main results are:

- Three types of slip markings were classified for the first time in terms of their morphology, their spatial distribution in the polycrystalline material and the stress amplitude ranges at which they appear predominantly.
- For stress amplitudes ranging from 45 MPa to 65 MPa, straight and long early persistent slip markings of type II are produced and located at twin boundaries oriented at about 45° from the loading direction. They are sometimes found in the HCF regime.
- For stress amplitudes below 45 MPa, clusters of fine and short early persistent slip markings of type III are produced and mainly located at triple junctions. They are rarely observed in HCF.
- The type III persistent slip markings are suggested to change into the type I or type II due to plastic strain localization mechanisms.
- Similar mechanisms are responsible for formation of persistent slip markings SBs at 20 kHz and frequencies lower than 100 Hz but do not take place in the same stress amplitude – number of cycles range.

- Results in VHCF demonstrated that when the stress amplitude decreases, the number of cycle to failure and the number of cycle needed to form persistent slip markings increases, and no limits are observed.
- The mechanical state responsible for the location of the three SM types will be investigated in another paper.

Acknowledgements

We would like to acknowledge the Agence Nationale de la Recherche France ANR-09-BLAN-0025-01 for the funding that enabled this work to be carried out and Camille Pissinier and Fabrice Détrez for their help in AFM measurements.

References

[1] Bathias C, Paris PC. Gigacycle fatigue in mechanical practice. New York: Marcel Dekker; 2005.
[2] Wang Q, Berard JY, Dubarre A, Baudry G G, Rathery S, Bathias C. Gigacycle fatigue of ferrous alloys. Fatigue Fract Eng Mater Struct 1999;22:667–72.
[3] Papakyriacou M, Mayer H, Pypen C, Plenk Jr H, Stanzl-Tschegg S. Influence of loading frequency on high cycle fatigue properties of b.c.c. and h.c.p. metals. Mater Sci Eng, A 2001;308:143–52.
[4] Stanzl-Tschegg S, Mayer H. Fatigue and fatigue crack growth of aluminium alloys at very high numbers of cycles. Int J Fatigue 2001;23:S231–7.
[5] Awatani J, Katagiri K, Omura A, Shiraishi T. A study of the fatigue limit of copper. Metal Trans 1975;6A:1029–34.
[6] Lukas P, Klesnil M, Polak J. High cycles fatigue life of metals. Mater Sci Eng 1974;15:239–45.
[7] Mughrabi H. In: Fatigue mechanisms in the ultrahigh cycle regime. Fatigue 2006. Atlanta; 2006.
[8] Mughrabi H. On multi-stage fatigue life diagrams and the relevant life controlling mechanisms in ultrahigh-cycle fatigue. Fatigue Fract Eng Mater Struct 2002;25:755–64.
[9] Hessler W, Müllner H, Weiss B, Stickler R. Near-threshold behaviour of polycrystalline copper. Met Sci 1981;15:225–30.
[10] Stanzl-Tschegg S, Mughrabi H, Schönbauer B. Life-time and cyclic slip of copper in the VHCF-regime. Int J Fatigue 2007:2050–9.
[11] Weidner A, Amberger D, Pyczak F, Schönbauer B, Stanzl-Tschegg S, Mughrabi H. Fatigue damage in copper polycrystals subjected to ultrahigh-cycle fatigue below the PSB threshold. Int J Fatigue 2010;32:872–8.
[12] Stanzl-Tchegg SE, Schönbauer B. Mechanisms of strain localization, crack initiation and fracture of polycrystalline copper in the VHCF regime. Int J Fatigue 2010;32:886–93.
[13] Krupp U, Knobbe H, Christ HJ, Köster P, Fritzen CP. The significance of microstructural barriers during fatigue of a duplex steel in the high- and very-high-cycle-fatigue (HCF/VHCF) regime. Int J Fatigue 2010;32:914–20.
[14] Höppel HW, May L, Prell M, Göken M. Influence of grain size and precipitation state on the fatigue lives and deformation mechanisms of CP aluminium and AA6082 in the VHCF-regime. Int J Fatigue 2011;33:10–8.
[15] Mughrabi H. On the life-controlling microstructural fatigue mechanisms in ductile metals and alloys in the gigacycle regime. Fatigue Fract Eng Mater Struct 1999;22:633–41.
[16] Cartensen JV, Mayer H, Bronsted P. Very high cycle fatigue of thin walled tubes made from austenitic stainless steel. Fatigue Eng Mater Struct 2002;25:37–844.
[17] Provan JW, Zhai ZH. Fatigue crack initiation and stage I propagation in polycrystalline materials I: Micromechanisms. Int J Fatigue 1991;13:99–109.
[18] Cretegny L, Saxena A. AFM characterization of the evolution of surface deformation during fatigue in polycrystalline copper. Acta Mater 2001;49:3755–65.
[19] Mughrabi H, Wang R, Differt K, Essman U. Fatigue crack initiation by cyclic slip irreversibilities in high-cycle fatigue. In: Lankford J, Davidson DL, Morris WL, Wei RPO, editors. Philadelphie: ASTM STP 811, American Society for Testing and Materials; 1983. p. 169–93.
[20] Kim WH, Laird C. Crack nucleation and stage I propagation in high strain fatigue-I. Microscopic and interferometric observations. Acta Metal 1998;26:777–87.
[21] Figueroa JC, Laird C. Crack initiation mechanisms in copper polycrystals cycled under strain amplitudes and in step tests. Mater Sci Eng 1983;60:45–58.
[22] Zhang P, Qu S, Duan Q, Wu S, Li S, Wang Z, et al. low-cycle fatigue cracking mechanisms in fcc crystalline materials. Philos Mag 2010;91:229–49.
[23] Ma B, Laird C. Overview of fatigue behaviour in copper single crystals-II population, size distribution and growth kinetics of stage I cracks for tests at constant amplitude. Acta Metal 1989;37:325–36.
[24] Neumann P, Tonnessen A. Crack initiation at grain boundaries in FCC materials – strength of metals and alloys, vol. 1. Oxfoxd: Pergamon Press; 1988.
[25] Pineau A, Antolovich S. Fatigue intergranulaire, dans Joints de grain et plasticité cristalline, sous la direction de Louisette Priester. Collection Traité Mécanique et Ingénierie des Matériaux. Hermès–Lavoisier: Série Matériaux et Métallurgie; 2011. p. 225–88 [chapitre 5].
[26] Polak J, Vasek A. Fatigue damage in polycrystalline copper below the fatigue limit. Vasek: Butterworth-Heinemann publisher; 1994.
[27] Mughrabi H. Dislocations and properties of real materials (Conf. Proc.), Book no. 323. London: The Institute of Metals; 1984. p. 244–60.
[28] Laufer EE, Roberts WN. Dislocation structures in fatigued copper single crystals. Philos Mag 1964;10:883–5.
[29] Mughrabi H, Wang R. Cyclic deformation of face-centred cubic polycrystals: a comparison with observations on single crystals. Deformation of polycrystals: mechanisms and microstructures. In: Hansen et al. N, editor. Proceedings of 2nd risø international symposium on metallurgy and materials science. Roskilde: Risø National Laboratory; 1981. p. 87–98.
[30] Peralta P, Laird C, Mitchell TE. Fatigue fracture at copper bicrystal interfaces: fractography. Mater. Sci. Eng 1999;A264:215–31.
[31] Llanes L, Laird C. The role of annealing twin boundaries in the cyclic deformation of f.c.c. materials. Mater Sci Eng, A 1992;157:21–7.
[32] Man J, Vystavěl T, Weidner A, Kuběna I, Petrenec M, Kruml T, et al. Study of cyclic strain localization and fatigue crack initiation using FIB technique. Int J Fatigue 2012;39:44–53.
[33] Thompson N, Wadsworth N, Louat N. The origin of fatigue fracture in copper. Philos Mag A 1956;1:113–26.
[34] Basinski SJ, Basinski ZS, Howie A. Early stages of fatigue in copper single crystals. Philos Mag A 1969;19:899–924.
[35] Risbet M, Feaugas X. Some comments about fatigue crack initiation in relation to cyclic slip irreversibility. Eng Fract Mech 2008;75:3511–9.
[36] Blanche A, Chrysochoos A, Ranc N, Favier V. Dissipation assessments during dynamic very high cycle fatigue. Exp Mech 2013 [accepted].